NASA TECHNICAL NOTE

NASA TN D-2832

NASA TN D-2832

DISTRIBUTION STATEMENT A
Approved for Public Release
Distribution Unlimited

AFTAC

BO 61071

EXPERIMENTAL INVESTIGATION OF HOT-GAS SIDE HEAT-TRANSFER RATES FOR A HYDROGEN-OXYGEN ROCKET

by Ralph L. Schacht, Richard J. Quentmeyer, and William L. Jones

Lewis Research Center
Cleveland, Ohio

20010906 047

REPRODUCED FROM BEST AVAILABLE COPY

NATIONAL AERONAUTICS AND SPACE ADMINIS[illegible]INGTON, D. C. • JUNE 1965

NASA TN D-2832

EXPERIMENTAL INVESTIGATION OF HOT-GAS SIDE HEAT-TRANSFER RATES FOR A HYDROGEN-OXYGEN ROCKET

By Ralph L. Schacht, Richard J. Quentmeyer, and William L. Jones

Lewis Research Center
Cleveland, Ohio

NATIONAL AERONAUTICS AND SPACE ADMINISTRATION

For sale by the Clearinghouse for Federal Scientific and Technical Information
Springfield, Virginia 22151 – Price $1.00

EXPERIMENTAL INVESTIGATION OF HOT-GAS SIDE HEAT-TRANSFER RATES FOR A HYDROGEN-OXYGEN ROCKET

by Ralph L. Schacht, Richard J. Quentmeyer, and William L. Jones

Lewis Research Center

SUMMARY

An experimental investigation was conducted at the Lewis Research Center to determine the hot-gas side heat-transfer rates in a rocket nozzle. Transient temperature measurements were made at five axial locations in a copper heat-sink nozzle having expansion and contraction area ratios of 4.64 with gaseous hydrogen and liquid oxygen as propellants. The nozzle was operated over a range of chamber pressures from 150 to 1000 pounds per square inch absolute at fuel percentages of 11 to 17, with most measurements made at approximately 15 percent hydrogen by weight.

The data are presented in a correlation equation of the form $St^*Pr^{*0.7} = CRe_d^{*-0.2}$, where St^*, Pr^*, and Re_d^* are reference Stanton, Prandtl, and Reynolds numbers, respectively, and C is a constant. Over the Reynolds number range investigated, the results showed that no one constant C correlates the data for all axial locations; however, the data did correlate well when each station was handled separately. The values of C varies from a high of 0.026 in the chamber to a low of 0.015 at the throat. This throat value is 42 percent lower than the widely used value of $C = 0.026$.

INTRODUCTION

In the design of convectively cooled nozzles for high-performance chemical and nuclear rocket systems the high heat fluxes and associated high wall temperatures require accurate knowledge of the heat flow across the gas boundary. Present design procedures involve gas-side heat-transfer correlations which have not been well substantiated by rocket heat-transfer data. Rocket-nozzle heat-transfer investigations are reported in references 1 to 5. Although the data of references 1 to 5 appear to correlate moderately well, the chamber pressure range, propellant combination, nozzle geometry, and instrumentation technique limit the usefulness of the data.

It was therefore deemed desirable to conduct a gas-side heat-transfer experiment over a wide range of chamber pressures with emphasis on the accurate determination of gas-side heat-transfer rates in the regime of high heat flux. Although this program is directed toward the solution of problems associated with both the cooling side and the hot-gas side, the investigation reported herein had the objective of providing useful hot-gas-side design information.

The rocket nozzle used for this investigation had a 5-inch-diameter throat with a 4.64 expansion and contraction area ratio. The propellants used were gaseous hydrogen and liquid oxygen. The nozzle wall was constructed of copper, which provided heat-sink cooling for the transiently conducted tests. Local heat-transfer rates were determined at five axial stations through the nozzle by transient temperature measurements using instrumented copper rods. The range of chamber pressures covered was approximately 150 to 1000 pounds per square inch absolute. The range of mixture ratios investigated corresponded to 11 to 17 percent hydrogen by weight, with the bulk of the runs being made at 15 percent hydrogen.

APPARATUS AND EXPERIMENTAL PROCEDURE

Rocket Design

A copper heat-sink, solid-wall, hydrogen-oxygen rocket was used in the experiments to obtain transient temperature data (fig. 1). The nozzle had a 4.64 contraction and ex-

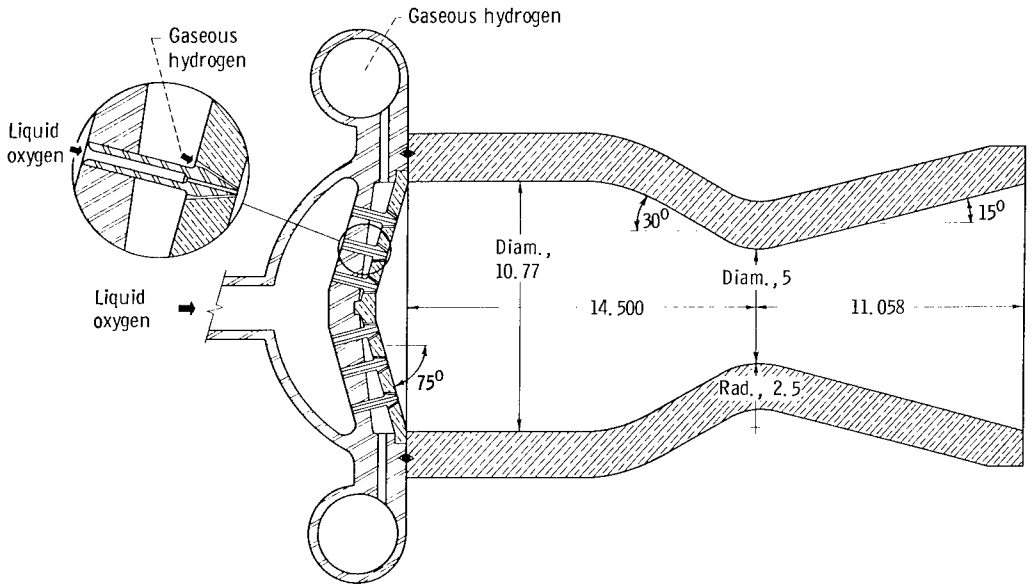

Figure 1. - Copper heat-sink rocket nozzle with coaxial injector. Dimensions given in inches.

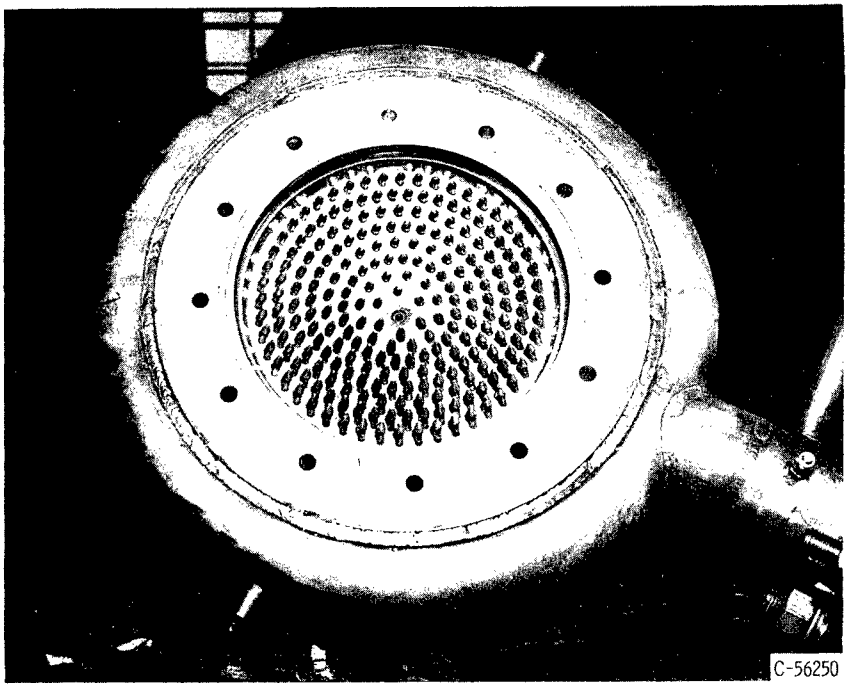

(a) Injector without faceplate.

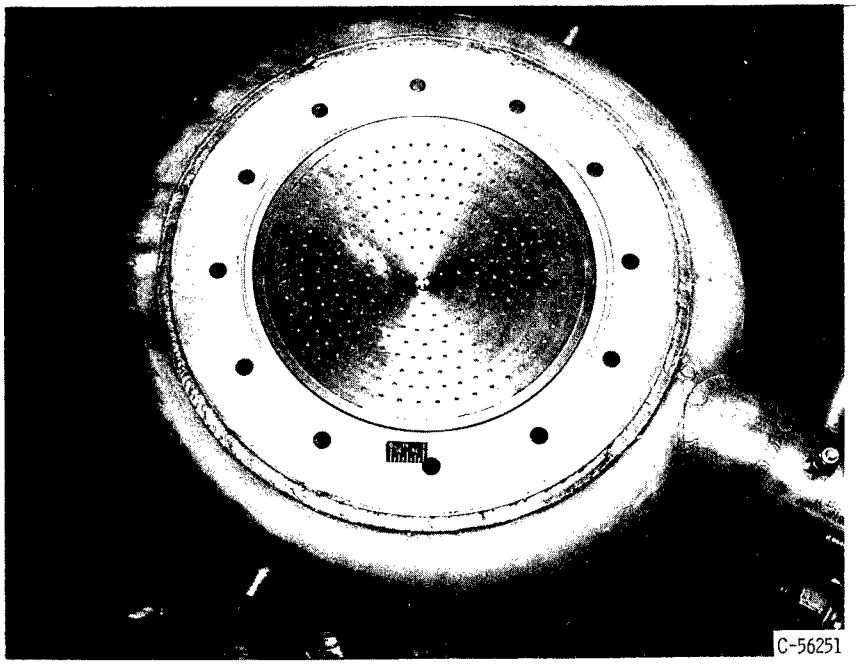

(b) Injector with copper faceplate.

Figure 2. - Coaxial 234 element injector.

pansion area ratio. The length of the combustion chamber from the injector to the throat was 14.5 inches. The characteristic length L^* was 54 inches. The throat diameter was 5 inches. The rocket developed 26 000 pounds of thrust at a chamber pressure of 900 pounds per square inch absolute.

A coaxial injector (figs. 1 and 2) was used with liquid oxygen and gaseous hydrogen as the propellants. The injector had 234 injector elements uniformly spaced in a dish-shaped faceplate (2.6 elements per square inch). Both chamber and injector were designed with the idea of obtaining stable engine operation and as uniform a distribution of mass flux and temperature as possible to eliminate striation effects.

Instrumentation

A small copper plug or rod was devised that, when inserted in the wall of the un-

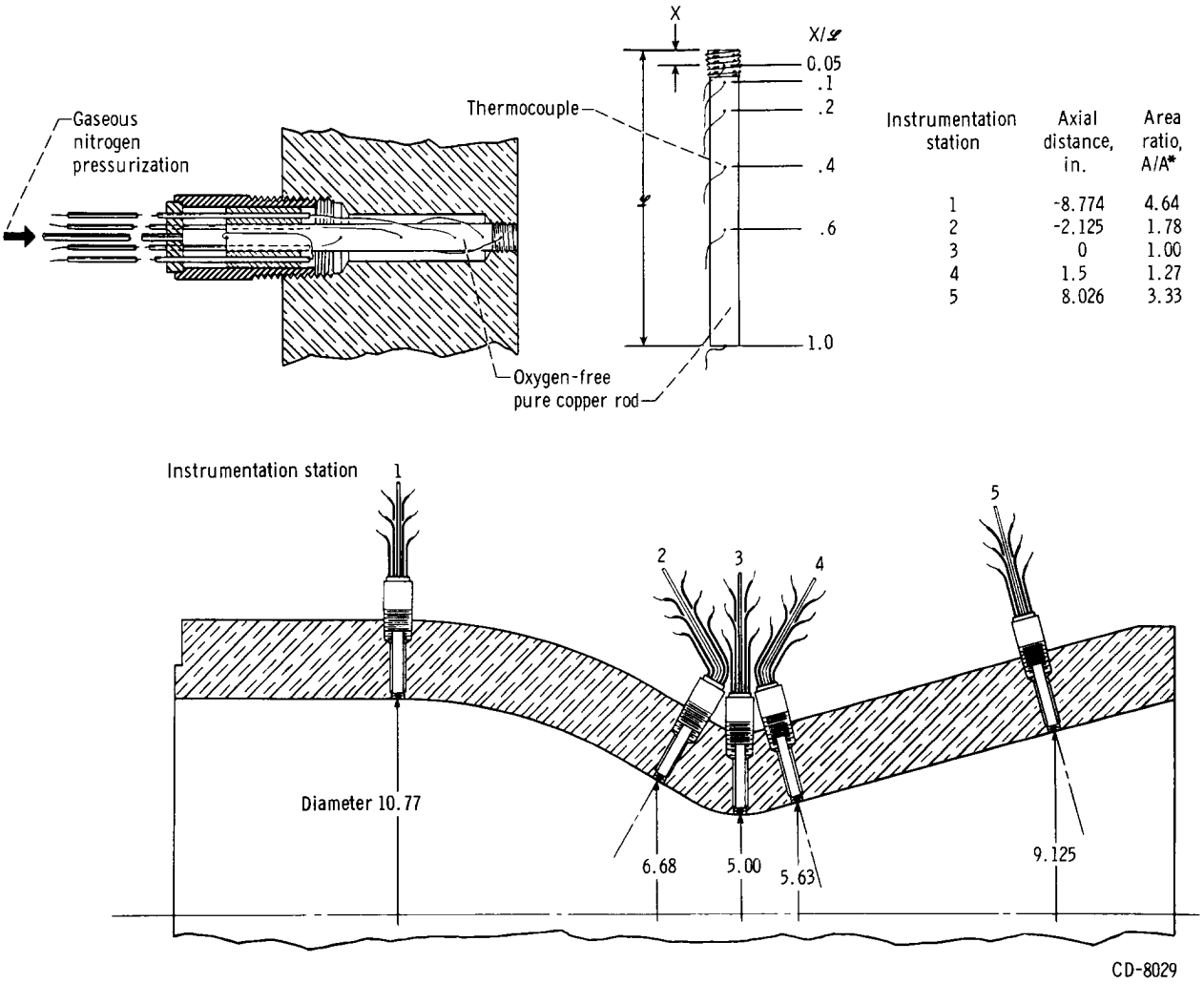

Instrumentation station	Axial distance, in.	Area ratio, A/A*
1	-8.774	4.64
2	-2.125	1.78
3	0	1.00
4	1.5	1.27
5	8.026	3.33

Figure 3. - Instrumentation locations and sealing details.

cooled rocket engine, approximated the model of a one-dimensional semi-infinite slab. As shown in figure 3, holes were machined normal to the inside wall of the copper nozzle at each of the seven measuring stations (five axial locations and two additional circumferential locations at the throat). Rods of pure, oxygen-free copper with diameters of 0.25 inch were used. The rods were threaded at the end for insertion in the machined holes. The threaded portion was machined so that its cross-sectional area closely approximated that of the 0.25-inch-diameter rod. This threaded portion was oxidized before insertion to minimize conduction between the rod and the chamber. The length of the rods was 2.5 inches, and the thickness of the chamber wall 2 inches. This length was picked to minimize the temperature differential between the heat-transfer surface of the rod and the surrounding chamber wall because of the larger volume of a radial element compared to the volume of the rod.

Figure 3 also shows the thermocouple stations on the copper rod. Six Chromel-Alumel thermocouples were used. The Chromel and Alumel wires, 0.008 inch in diameter, were peened to the surface. Figure 3 shows a detail of the sealing method used at the end of the rod. The cavity surrounding the rod was pressurized with room-temperature nitrogen to a pressure 5 to 10 percent below that of the local static pressure at each measuring station to prevent hot gas leakage past the threaded portion of the rod. The pressures were monitored during each run to ensure that no film cooling was obtained from the pressurizing gas. Cavity pressure remained constant with time after the start of a run.

Data Recording

Propellant flow, chamber pressure, and rod temperatures were recorded in a digitized form on a magnetic tape for direct entry into a digital computer. The digital recording system had basic sampling rates of 4000 words per second. Figure 4 (p. 6) shows the basic block of data as taken by the digitizer. Most data parameters were arranged in the block so that, with a minimum of five blocks of data, 60-cycle noise could be defined. Then a smoothing technique was used to eliminate the 60-cycle noise and greatly diminish any random noise. The calculating procedure fit a smooth curve through 15 readings of the data parameter, and then one report, to be used in the terminal calculations, was made for all parameters at a common time. This reduced the amount of terminal calculations. Chamber pressure, which was sampled nine times in each block, was used as a triggering device for starting and stopping the calculations.

Full scale, mV	Amplifier	Word number							
		0-7	8-15	16-23	24-31	32-39	40-47	48-55	56-63
20	0	P_c	P_{H_2orf}	P_c	$T_{3A,1}$	P_c	P_c	P_{H_2orf}	P_c
20	1	T_{H_2orf}	ΔP_{H_2orf}	$\dot{w}_{O_2}$	$T_{3A,2}$	$T_{3B,1}$	T_{H_2orf}	ΔP_{H_2orf}	$\dot{w}_{O_2}$
50	2	$T_{1,1}$	$T_{2,1}$	$T_{3,1}$	$T_{4,1}$	$T_{5,1}$	$T_{1,1}$	$T_{2,1}$	$T_{3,1}$
50	3	$T_{1,2}$	$T_{2,2}$	$T_{3,2}$	$T_{4,2}$	$T_{5,2}$	$T_{1,2}$	$T_{2,2}$	$T_{3,2}$
50	4	$T_{1,3}$	$T_{2,3}$	$T_{3,3}$	$T_{4,3}$	$T_{5,3}$	$T_{1,3}$	$T_{2,3}$	$T_{3,3}$
50	5	$T_{1,4}$	$T_{2,4}$	$T_{3,4}$	$T_{4,4}$	$T_{5,4}$	$T_{1,4}$	$T_{2,4}$	$T_{3,4}$
50	6	$T_{1,5}$	$T_{2,5}$	$T_{3,5}$	$T_{4,5}$	$T_{5,5}$	$T_{1,5}$	$T_{2,5}$	$T_{3,5}$
50	7	$T_{1,6}$	$T_{2,6}$	$T_{3,6}$	$T_{4,6}$	$T_{5,6}$	$T_{1,6}$	$T_{2,6}$	$T_{3,6}$

Full scale, mV	Amplifier	Word number							
		64-71	72-79	80-87	88-95	96-103	104-111	112-119	120-127
20	0	$T_{3A,1}$	P_c	P_c	P_{H_2orf}	P_c	$T_{3A,1}$	P_c	$T_{3A,3}$
20	1	$T_{3A,2}$	$T_{3B,1}$	T_{H_2orf}	ΔP_{H_2orf}	$\dot{w}_{O_2}$	$T_{3A,2}$	$T_{3B,1}$	$T_{3A,4}$
50	2	$T_{4,1}$	$T_{5,1}$	$T_{1,1}$	$T_{2,1}$	$T_{3,1}$	$T_{4,1}$	$T_{5,1}$	$T_{3B,1}$
50	3	$T_{4,2}$	$T_{5,2}$	$T_{1,2}$	$T_{2,2}$	$T_{3,2}$	$T_{4,2}$	$T_{5,2}$	$T_{3B,2}$
50	4	$T_{4,3}$	$T_{5,3}$	$T_{1,3}$	$T_{2,3}$	$T_{3,3}$	$T_{4,3}$	$T_{5,3}$	$T_{3B,3}$
50	5	$T_{4,4}$	$T_{5,4}$	$T_{1,4}$	$T_{2,4}$	$T_{3,4}$	$T_{4,4}$	$T_{5,4}$	$T_{3B,4}$
50	6	$T_{4,5}$	$T_{5,5}$	$T_{1,5}$	$T_{2,5}$	$T_{3,5}$	$T_{4,5}$	$T_{5,5}$	$T_{3B,5}$
50	7	$T_{4,6}$	$T_{5,6}$	$T_{1,6}$	$T_{2,6}$	$T_{3,6}$	$T_{4,6}$	$T_{5,6}$	$T_{3B,6}$

First subscript denotes station; second subscript denotes X/ℓ location.

Figure 4. - Digitizer data block.

Test Procedure

The rocket engine (fig. 5) was installed on a test stand located at the Lewis Plum Brook Facility. Propellant valves for controlling gaseous hydrogen and liquid oxygen were prepositioned before the run and opened to these fixed positions during the run to provide the desired values for chamber pressure and percent of hydrogen. Chamber pressures were varied from 150 to 1000 pounds per square inch absolute at 11 to 17 percent hydrogen. The timing and sequencing of the valves were adjusted so that full chamber pressure was obtained in 0.02 to 0.06 second for a typical run as shown in figure 6. This step function in chamber pressure or driving temperature allowed a simpler mathematical model to be used for obtaining heat-transfer coefficients.

CALCULATION PROCEDURE

Constant h Method

The differential equation for one-dimensional heat conduction in a homogeneous medium is

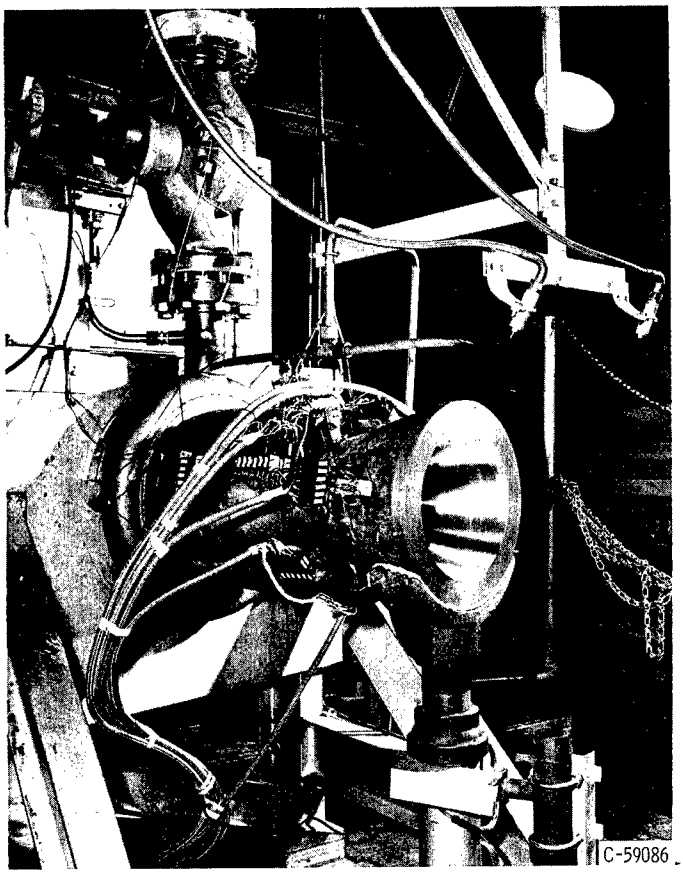

Figure 5. - Copper heat-sink nozzle installed in test facility.

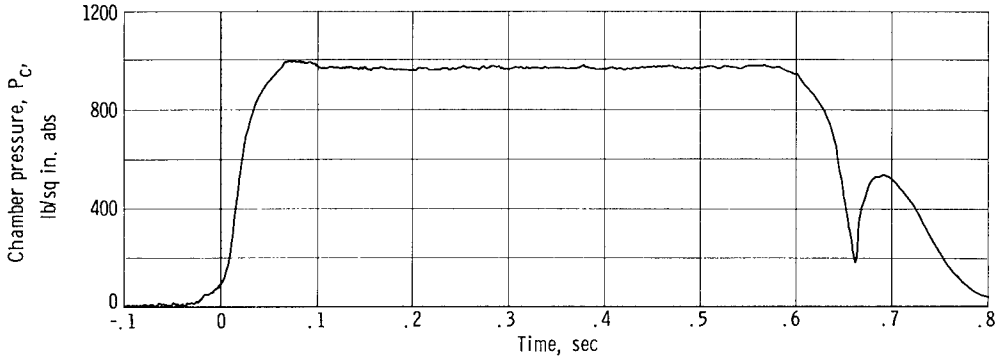

Figure 6. - Typical oscillograph trace of chamber pressure against time.

$$k\frac{\partial^2 T}{\partial X^2} = \rho c \frac{\partial T}{\partial t} \tag{1}$$

with the boundary conditions

$$-k\frac{\partial T}{\partial X} = h(T_{aw} - T) \qquad \text{at } X = 0 \tag{2}$$

$$k\frac{\partial T}{\partial X} = 0 \qquad \text{at } X = \mathscr{L} = \infty \tag{3}$$

The initial condition is $T = T_0$ at $t = 0$. (Symbols are defined in the appendix.) The assumption that the heat-transfer rates are proportional to the difference between the temperature at the wall and the temperature of the surrounding medium (eq. (2)) seems to be justified because the heat transfer occurs primarily by convection, rather than conduction or radiation. Radiant heat transfer is estimated to be an order of magnitude less than that due to convection for this experiment. It is therefore neglected in the theoretical treatment. The measurements, however, include both effects. The solution to equation (1) is given in closed form in reference 6.

Reference 7 has put this solution in the form

$$\varphi(N_X, \tau^*) = \operatorname{erfc}\frac{N_X}{2\sqrt{\tau^*}} - e^{(N_X+\tau^*)}\operatorname{erfc}\left(\frac{N_X}{2\sqrt{\tau^*}} + \sqrt{\tau^*}\right) \tag{4}$$

where

$$\operatorname{erfc} z = 1 - \frac{2}{\sqrt{\pi}}\int_0^z e^{-z^2}\,dz$$

while the dimensionless variables are

$$\varphi = \frac{T - T_0}{T_{aw} - T_0}$$

$$N_X = \frac{hX}{k}$$

$$\tau^* = \frac{h^2 t}{k\rho c}$$

Equation (4) has the factor 2 added, which was erroneously omitted in reference 7.

Equation (4) holds until such time as the temperature starts to rise at the position $X = \mathscr{L}$ (the thickness of the slab). For shorter times the temperature distribution given by equation (4) is approximately represented by that in a semi-infinite solid, the accuracy increasing as $X = \xi\mathscr{L}$ approaches the hot boundary ($\xi \to 0$).

When the temperature starts to rise at $X = \mathscr{L}$, equation (4) fails because of boundary condition (eq. (3)). Since longer running times are needed, this failure of the solution can be remedied by allowing, in addition to the heat source of strength $h(T_{aw} - T)$ at $X = 0$, an additional heat source of this strength at $X = 2\mathscr{L}$. Reference 7 shows that, with two identical sources located symmetrically about $X = \mathscr{L}$, the conduction of heat in the region $0 \leq X \leq \mathscr{L}$ is governed by the same differential equation and initial boundary conditions as in the slab, but the solution given applies during the time when the temperature at $X = 0$ is not influenced by the image source at $X = 2\mathscr{L}$. The temperature of the slab is therefore accurately represented within this extended time period by the superimposed effect of the two sources:

$$\varphi\left(N_X, \tau^*\right) = \varphi\left(N_{X=\xi\mathscr{L}}, \tau^*\right) + \varphi\left[N_{X=(2-\xi)\mathscr{L}}, \tau^*\right] \tag{5}$$

Equation (5) was programed on a digital computer so that an iteration process found the h that satisfied the measured φ for a given location ξ and time τ^*. The last term, $\varphi[N_{X=(2-\xi)\mathscr{L}}, \tau^*]$, was also reported so that cutoff of data could be made when the temperature rise at $X = 0$ was not yet influenced by the image source at $X = 2\mathscr{L}$. Since the engine runs were all necessarily of short duration, equation (5) was sufficient for reduction of the data.

The properties of materials (k, ρ, and c) may vary appreciably with temperature, and a problem arises concerning which temperature in the material should be used in the evaluation. Reference 8 shows that the material properties for simple metals for this type of computation should be evaluated at a temperature that is about one-fourth of the maximum if the initial temperature is zero, or at $(T_{\xi=0} - T_0)/4 + T_0$ if the initial tem-

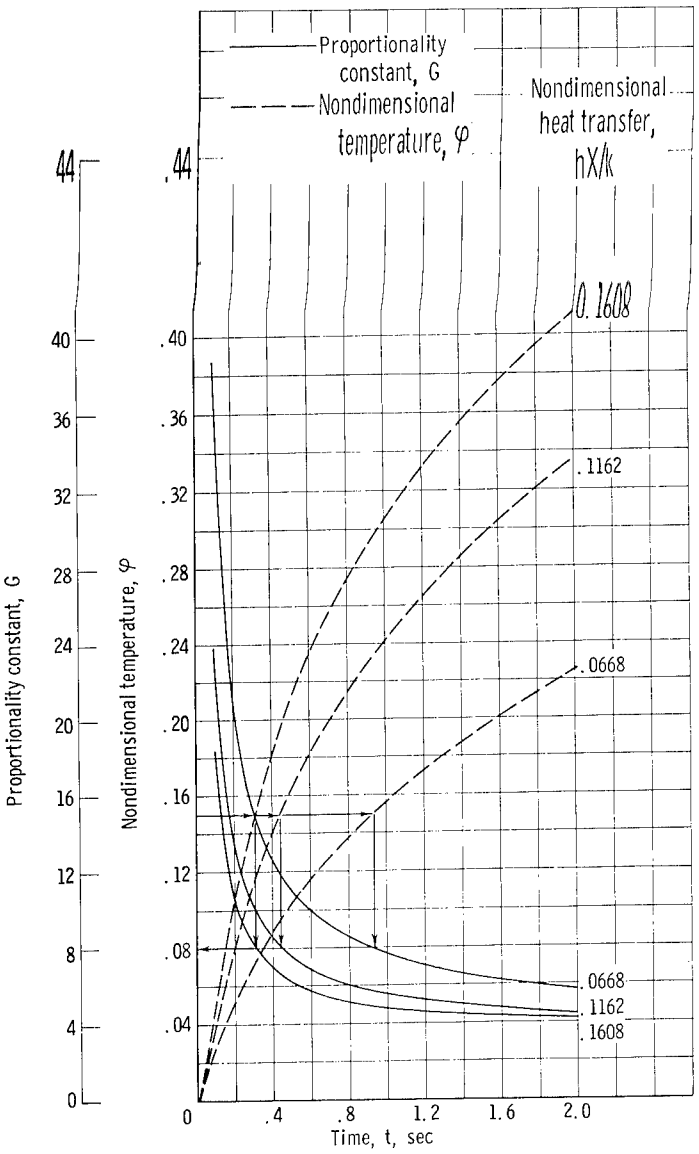

Figure 7. - Proportionality constant and nondimensional temperature as functions of time. Distance normal to heated surface, 0.125 inch; k/ρc, 0.001151 square foot per second.

perature is nonzero. The temperature of the rod at $\xi = 0$ was approximated with finite differences by the equation

$$T_{\xi=0} = \frac{8}{3} T_{\xi=0.05} - 2 T_{\xi=0.1} + \frac{1}{3} T_{\xi=0.2}$$

where $T_{\xi=0.05}$, $T_{\xi=0.1}$, and $T_{\xi=0.2}$ are measured values.

Figure 7 shows the results of a study that relates the error in a nondimensional temperature φ to the percent error in the nondimensional heat transfer hX/k. The nondimensional temperature φ is plotted against time for various hX/k values. The proportionality constant G from the equation

$$\frac{d(hX/k)}{hX/k} = G \, d\varphi$$

is plotted against time for the same hX/k values. Since the limit of running time for a heat-sink engine is a constant value of φ (T_w close to melting at the surface), it can be seen from figure 7 that G remains essentially constant with hX/k. Thus, even though the length of running time goes down as chamber pressure is increased (hX/k is increased), the accuracy of obtaining h remains the same for a given measurement inaccuracy $d\varphi$ and a constant φ. If the accuracy in obtaining φ is estimated to be ±5 percent in the range of $\varphi = 0.15$, the percent error in hX/k is ±8 (0.15) (0.05) (100) or ±6.0 percent, as shown by arrow in figure 7.

Integration Method

An integration method was also used to check the results from the constant h method

described. If the slab is considered to be insulated on all surfaces except the heat-transfer surface, the time rate of change of the integrated heat content must be equal to the rate of heat flow through the surfaces:

$$q = \frac{1}{A}\frac{\partial}{\partial t}\int_0^{\mathscr{L}} A_X Q_X \, dX = \frac{1}{A}\frac{\partial}{\partial t}\int_0^{\mathscr{L}} (\rho A c T)_X \, dX \tag{6}$$

In equation (6) the heat content Q_X is above some arbitrary reference level. If the slab cross-sectional area is constant over its length, the area term does not appear in equation (6). If a short time increment after the start of steady-state burning is considered, the time rate of change of integrated heat content at the arithmetic average of these two times is equal to the difference in heat content divided by the time interval. The heat-transfer coefficient can be obtained from the following equation:

$$h_{0.5(t_1+t_2)} = \frac{1}{(T_{aw} - T_w)_{0.5(t_1+t_2)}} \left\{ \frac{1}{t_2 - t_1} \left[\int_0^{\mathscr{L}} (\rho c T)_{t_2} \, dX - \int_0^{\mathscr{L}} (\rho c T)_{t_1} \, dX \right] \right\}$$

In this equation the ρc product is evaluated at the measured temperature at X.

Combustion Temperature

Before h can be computed by the methods described previously, the driving temperature (T_{aw}) must be determined throughout the nozzle; to determine T_{aw} the combustion temperature must be known. Combustion temperature is a function of combustion chamber pressure, percent fuel, and combustion efficiency.

Numerous programs are presently in existence for the calculation of equilibrium compositions and other thermodynamic properties of complex chemical systems. The programs of reference 9 for thermodynamic properties and of reference 10 for transport properties were modified and simplified for a gaseous-hydrogen - liquid-oxygen system by Frederic N. Goldberg of the NASA Lewis Research Center. The program was further modified to account for combustion efficiency. The procedure used to account for combustion efficiency and arrive at the proper combustion temperature is described in the paragraphs that follow.

Under the conditions of one-dimensional isentropic equilibrium flow, the specification of chamber enthalpy H_c (for a given mixture ratio), combustion chamber pressure P_c, and throat area per unit weight flow $(A/\dot{w})_{th}$ may lead to an incompatability. If the

calculated value of $(A/\dot{w})_{min}$ corresponding to the minimum value of the function $A/\dot{w} = f(P, S_c)$ (where S_c is the entropy of the chamber gases determined by H_c and P_c) differs from $(A/\dot{w})_{th}$, then one of the input specifications must be relaxed.

Since the measurements considered to be most reliable were those of combustion pressure and geometric throat area, these were considered to be invariant. When the calculated value $(A/\dot{w})_{min}$ was greater than $(A/\dot{w})_{th}$, an iteration was used to determine a chamber enthalpy, or equivalently a combustion temperature T_c, compatible with the measured weight flow and the requirement that choking occurs at the geometric throat according to the following algorithm:

$$\left(\frac{A}{\dot{w}}\right)_{min}^{K} = f\left(P, S_c^K\right)$$

$$T_c^{K+1} = T_c^K \left[\frac{\left(\frac{A}{\dot{w}}\right)_{th}}{\left(\frac{A}{\dot{w}}\right)_{min}^{K}}\right]^2$$

$$S_c^{K+1} = S\left(T_c^{K+1}, P_c\right)$$

where the $K = 0$ conditions correspond to those of specified input enthalpy. Calculations were terminated when there was sufficiently close agreement between the calculated and measured throat area per unit weight flow. The square root of the ratio of the final combustion temperature to $T_c^{K=0}$ was used as a measure of combustion efficiency.

If the initial calculated $(A/\dot{w})_{min}$ was less than that measured, the enthalpy was left invariant. (Note that in this case the preceding method would indicate an efficiency greater than 100 percent.) A new weight flow was then calculated with the combustion efficiency assumed to be 100 percent:

$$\dot{w}_{new} = \left[\frac{\left(\frac{A}{\dot{w}}\right)_{th}}{\left(\frac{A}{\dot{w}}\right)_{min}}\right] \dot{w}_{measured}$$

The average combustion efficiency obtained from all the test data was 98 percent of theoretical equilibrium.

Transport Properties

Eckert and Drake, in a summary discussing turbulent boundary layers (ref. 11), recommend that the transport properties appearing in the correlation equations be introduced at a reference enthalpy given by the equation

$$H^* = H_s + 0.5(H_w - H_s) + 0.22(Pr^*)^{1/3}(H_{tot} - H_s)$$

instead of by temperature when the range of temperature is such that the specific heat varies considerably within the boundary layer. Therefore, the nondimensional heat-transfer parameters were computed by introducing the transport properties as a function of H^* and P_s for the hydrogen-oxygen system described.

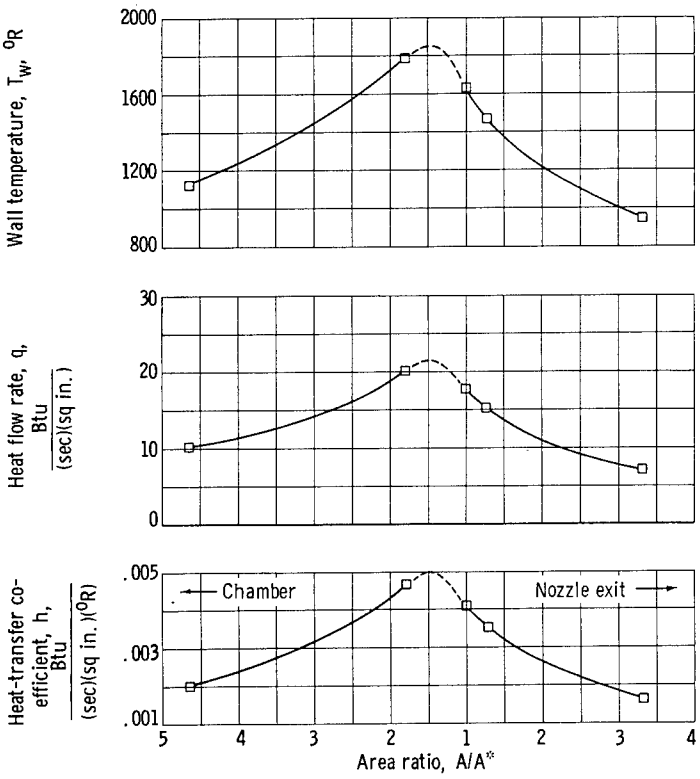

Figure 8. - Typical profiles of wall temperature, heat flow rate, and heat-transfer coefficient plotted against area ratio. Chamber pressure, 967 pounds per square inch absolute; fuel mixture, 16.5 percent hydrogen; time, 0.462 second.

RESULTS AND DISCUSSION

Figure 8 is a plot of the wall temperature, heat flux, and heat-transfer coefficient for a typical run, for which the chamber pressure was 967 pounds per square inch absolute, the hydrogen concentration was 16.5 percent, and the time 0.462 second. Figure 8 shows that the heat flux was indeed in the range of anticipated nuclear-rocket nozzles, that is, q = 20 Btu per square inch per second, and $T_w = 2000^o$ R.

The results presented in this report are all from the constant h solution. As running progressed, thermocouples at $X/\mathscr{L} = 0.6$ and $X/\mathscr{L} = 1.0$ were lost and the integration method could not be applied. For some of the earlier tests, however, results from the integration method agreed with the constant h solution and gave additional support

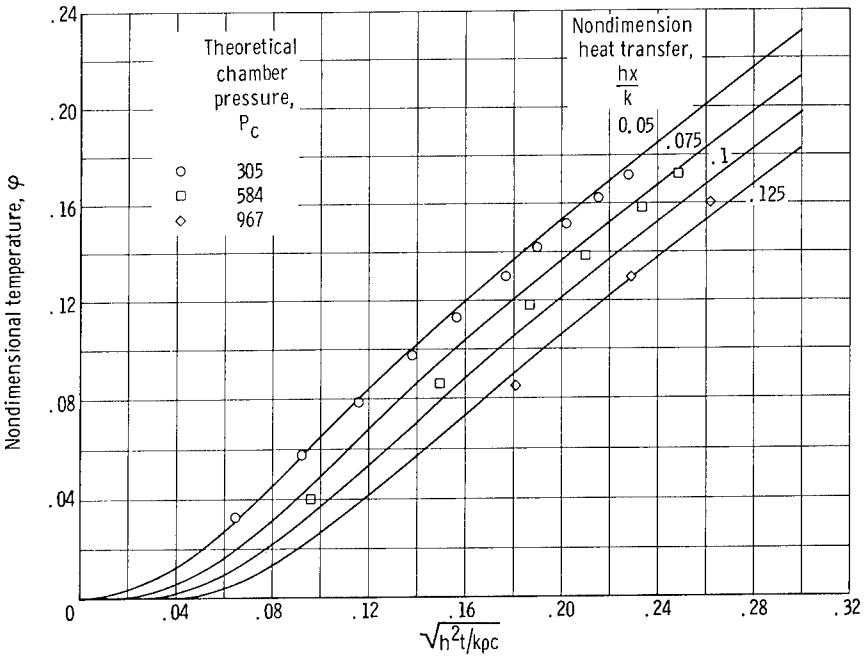

Figure 9. - Trend comparison of theoretical and measured temperature transients in semi-infinite solid. (x = 0.125 in.)

to this method. For a further test of the apparatus and technique a second nozzle fabricated and instrumented in the same manner was run at two of the chamber conditions. Data reproducibility was shown to be good; that is, it fell within the spread of the data and thus indicated nothing unique about one particular apparatus.

Before the results of any experiment can be used, the validity of the results must be established. Figure 9 can be used to consider the results. The solid lines are the theoretical lines from equation (4) rewritten as follows to include the pertinent variables

$$\varphi = \operatorname{erfc} \frac{\frac{hX}{k}}{2\sqrt{\frac{h^2t}{k\rho c}}} - e^{\left(\frac{hX}{k}+\frac{h^2t}{k\rho c}\right)} \operatorname{erfc}\left(\frac{\frac{hX}{k}}{2\sqrt{\frac{h^2t}{k\rho c}}} + \sqrt{\frac{h^2t}{k\rho c}}\right)$$

for $hX/k = 0.05$, 0.075, 0.1, and 0.125 and $X = 0.125$ inch. Experimental data from one thermocouple for the throat station are shown for three chamber pressures. The experimental points follow the contours of the theoretical lines fairly well; thus the assumption of a constant h solution and a one-dimensional model seems justified.

The data for the range of chamber pressures from 150 to 1000 pounds per square inch absolute are presented in figure 10 for each measuring station of the rocket nozzle.

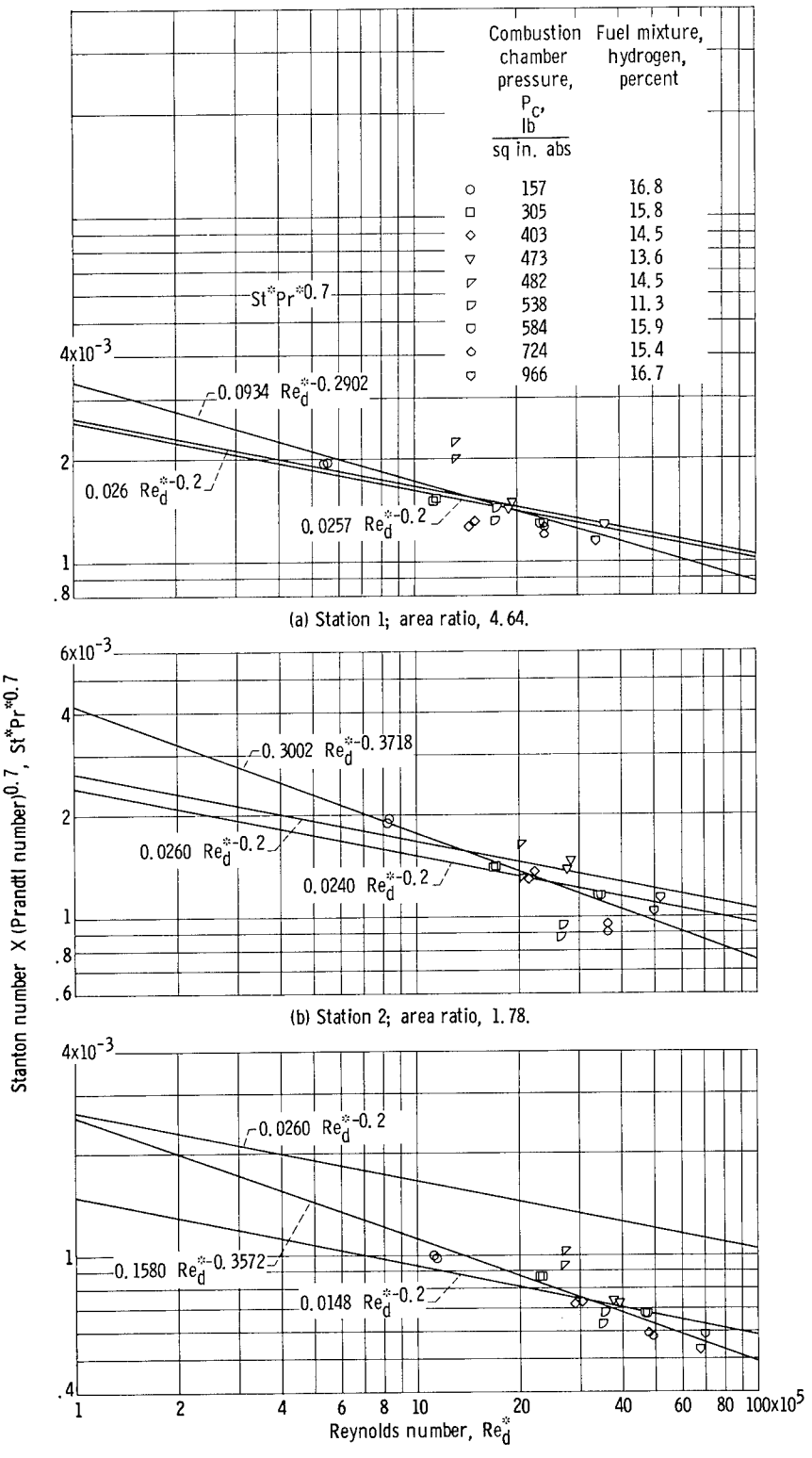

Figure 10. - Product of Stanton and Prandtl numbers as function of Reynolds number.

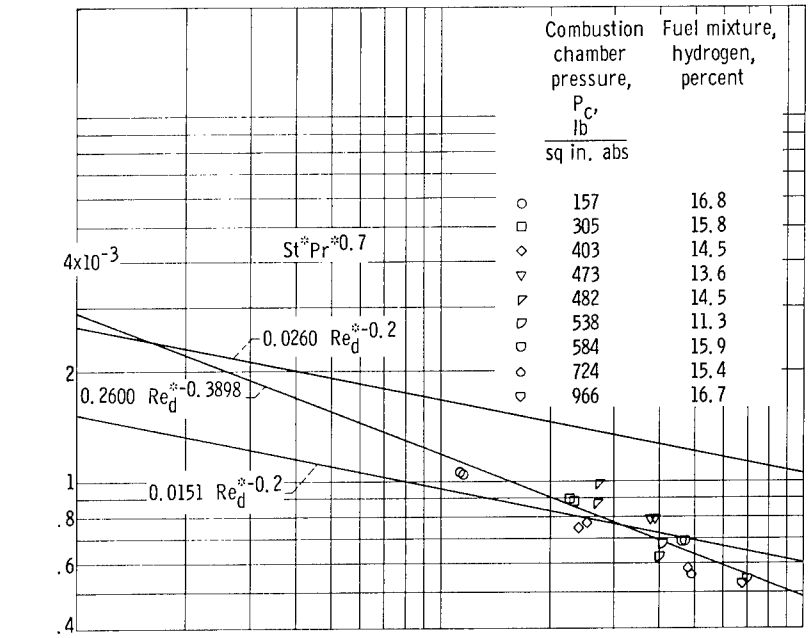

(d) Station 3; area ratio, 1.00 (average for three circumferential stations at throat).

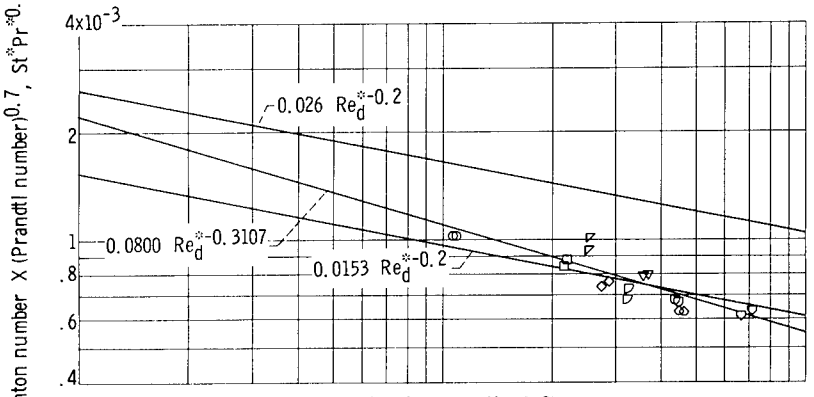

(e) Station 4; area ratio, 1.27.

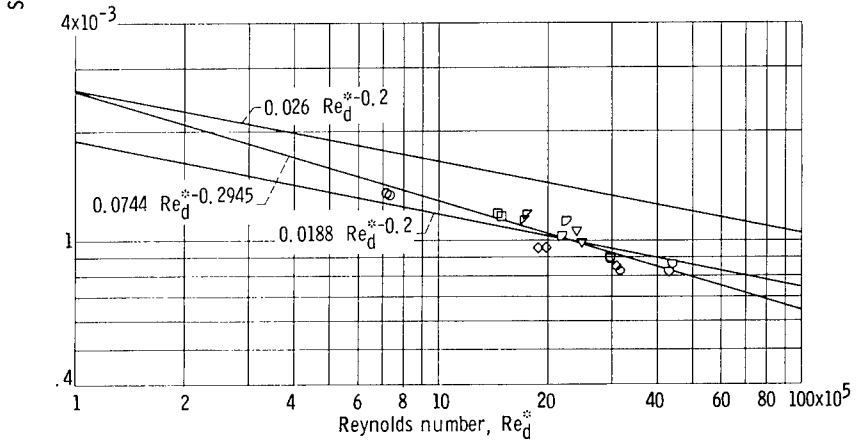

(f) Station 5; area ratio, 3.33.

Figure 10. - Concluded.

Figure	Station	Constant, C	Standard deviation, σ	$\frac{\sigma}{C} \times 100$, percent	1.96 σ	$\frac{1.96\,\sigma}{C} \times 100$, percent
10(a)	1	0.0257	0.0028	10.9	0.0056	21.8
10(b)	2	.0240	.0039	16.3	.0077	32.1
10(c)	3	.0148	.0020	13.5	.0039	26.3
10(d)	$\overline{3}$	.0151	.0020	13.2	.0039	25.8
10(e)	4	.0153	.0016	10.4	.0031	20.3
10(f)	5	.0188	.0015	7.9	.0030	16.0

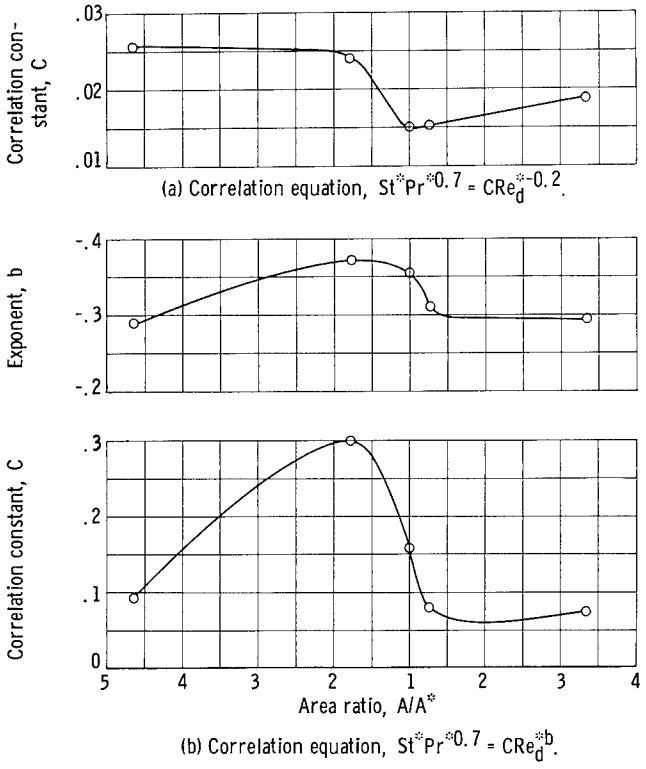

(a) Correlation equation, $St^*Pr^{*0.7} = CRe_d^{*-0.2}$.

(b) Correlation equation, $St^*Pr^{*0.7} = CRe_d^{*b}$.

Figure 11. - Exponent and correlation constant as functions of area ratio for two correlation equations.

Station $\overline{3}$ represents the average values for the three measuring stations at the throat (3, 3A, and 3B). The nondimensional parameter $St^*Pr^{*0.7}$ is plotted against Re_d^*. All transport properties were introduced at the reference enthalpy and static pressure for each station. Chemical equilibrium conditions were used. For these plots duplicate data points represent calculations made for each of the last two common time reports for each run. The last two time reports give the greatest $T - T_0$ input into the parameter $\varphi = (T - T_0)/(T_{aw} - T_0)$ and therefore have the least error, as shown by figure 7 (p. 10). Figure 9 shows that h is fairly constant with time.

In each part of figure 10 two least-square fits for the data are plotted, one where the constant and the exponent of the Reynolds number were both allowed to vary in the standard equation of the form $St^*Pr^{*0.7} = CRe_d^{*b}$, the other where only the constant is allowed to vary and the exponent b is held at a fixed value of -0.2. The constants and the exponents are shown for each curve. The plots also have the line represented by the equation $St^*Pr^{*0.7} = 0.026\,Re_d^{*-0.2}$, which is similar to the simplified Bartz equation (ref. 12).

In order to give a better statistical interpretation of the data spread around the much used $St^*Pr^{*0.7} = CRe_d^{*-0.2}$ correlation, the standard deviation and the percent deviation for each station are presented in the preceding table. The column headed 1.96 σ shows the deviation around C defining the 95 percent confidence interval.

Over the Reynolds number range covered by these experiments either correlation ($St^*Pr^{*0.7} = CRe_d^{*-0.2}$ or $St^*Pr^{*0.7} = CRe_d^{*b}$) seems to be adequate for obtaining heat-transfer coefficients at a given station for the hydrogen-oxygen system used.

Figure 11(a) is a plot of the constant against area ratio for an exponent of -0.2. These data indicate that no one value of C will correlate the data for all axial locations. In fact, the constant C = 0.026, which has been widely used to predict gas-side heat-transfer coefficients for nozzles, overpredicts the coefficients for all axial locations except the chamber. The measured heat-transfer coefficients at the throat were approximately 42 percent less than those predicted by the equation $St^*Pr^{*0.7} = 0.026\ Re_d^{*-0.2}$. Figure 11(b) shows plots of the exponent and the constant against area ratio where the curve fit of the data allowed both to vary.

From hydrogen-oxygen data presented in reference 5 for a chamber pressure of 150 pounds per square inch absolute and a mixture ratio of 5.0 (16.7 percent hydrogen), it was possible to compute values of the throat heat-transfer coefficient h. This computation gave a band of h from 0.0014 to 0.0010 Btu per square inch per second per $^{\circ}R$, which compares with a value of 0.00136 measured at the throat of the nozzle tested herein under the same operating conditions. Thus, the level of the heat-transfer coefficients at the throat shows reasonable agreement for the hydrogen-oxygen system at low chamber pressures.

Data taken from reference 3 for three nozzle configurations were recalculated using a reference enthalpy input of all transport properties and fitted to the equation $St^*Pr^{*0.7} = CRe_d^{*-0.2}$. The resulting C values at the throat were 0.019, 0.017, and 0.023, respectively. Data taken from reference 4 were recalculated in a similar manner, and a value of $C \simeq 0.018$ at the throat resulted. The curves of C against area ratio A/A^* also showed trends similar to those of figure 11 (i.e., values of C high in the chamber, low in the throat, and increasing again at the exit). A mention of this work is given only to say that, while the variation of C with A/A^* that was found is considered correct for the nozzle geometry, propellant system, and injectors used, the values should not be used universally for calculating the heat-transfer rate to other nozzles.

CONCLUDING REMARKS

If a designer desires to use the correlations presented herein for a system similar to the rocket of this experiment, he must work with the thermodynamic and transport properties for chemical equilibrium as computed herein (refs. 9 and 10). All properties must be inserted at the reference enthalpy and static pressure of the axial station where the heat-transfer coefficient is desired. The effect of using different properties can be

great. Using the new transport properties (ref. 10) reduced the correlation constant C by approximately 30 percent over those obtained by using transport properties from reference 13. Transport properties given in reference 10 are considered to be more accurate than those previously used.

The values of the correlation constant C reported herein are for a given nozzle geometry, propellant combination, and injector configuration and are not to be considered universal for rocket heat-transfer calculations.

SUMMARY OF RESULTS

An experimental investigation was conducted at the Lewis Research Center to determine the hot-gas-side heat-transfer rates in a rocket nozzle. Transient temperature measurements were made at five axial locations in a copper heat-sink nozzle with expansion and contraction ratios of 4.64 with gaseous hydrogen and liquid oxygen as propellants. The nozzle was operated over a range of chamber pressures from 150 to 1000 pounds per square inch absolute at fuel percentages ranging from 11 to 17, with most measurements made at approximately 15 percent hydrogen. The following results were obtained:

1. The data at a given location in the nozzle are adequately correlated by the equation $St^*Pr^{*0.7} = CRe_d^{*-0.2}$, where St^*, Pr^*, and Re_d^* are reference Stanton, Prandtl, and Reynolds numbers, respectively, and C is a constant.

2. The constant C varies with axial location and is less than 0.026 for all locations except the chamber.

3. The constant C at the throat was 42 percent less than the widely used value of $C = 0.026$.

Lewis Research Center,
National Aeronautics and Space Administration,
Cleveland, Ohio, March 16, 1965.

APPENDIX - SYMBOLS

A	cross-sectional area, sq in.
b	exponent in equation $St^{*}Pr^{*0.7} = CRe_d^{*b}$
C	constant in equation $St^{*}Pr^{*0.7} = CRe_d^{*b}$
c	specific heat of materials, Btu/(lb)(^{o}R)
G	proportionality constant; $d\left(\frac{hX}{k}\right)\Big/\frac{hX}{k} = G\, d\varphi$
H	enthalpy
H_{aw}	adiabatic wall enthalpy, $H_s + \sqrt[3]{Pr^*}\,(H_{tot} - H_s)$
h	heat-transfer coefficient, Btu/(sec)(sq in.)(^{o}R)
k	thermal coefficient of conductivity of material, Btu/(sec)(in.)(^{o}R)
L^*	characteristic length of rocket engine, in., V_c/A_{th}
$\mathscr{L}$	length of heat flow path in rod, in.
N_X	nondimensional parameter, hX/k
P	pressure, lb/sq in. abs
Pr	Prandtl number
Q	quantity of heat, Btu/cu in.
q	heat flow rate per unit area, Btu/(sec)(sq in.)
Re_d	Reynolds number based on diameter
S	entropy, Btu/(lb)(^{o}R)
St	Stanton number
T	temperature, ^{o}R
T_{aw}	$f(H_{aw}, P_s)$
t	time, sec
t_1	time 1, sec
t_2	time 2, sec
V	volume, cu in.
$\dot{w}$	total weight flow rate, lb/sec
$\dot{w}_{O_2}$	oxygen weight flow rate, lb/sec
X	distance normal to heat surface, in.
ξ	nondimensional parameter, $X/\mathscr{L}$
ρ	material density, lb/cu in.
σ	standard deviation
τ^*	nondimensional parameter, $h^2t/k\rho c$
φ	nondimensional temperature, $(T - T_0)/(T_{aw} - T_0)$
$\overline{3}$	average value for three circumferential measuring stations at throat of rocket (station 3)

Subscripts:

A, B	circumferential locations at throat (station 3, 120^{o} apart)
c	chamber
min	minimum
orf	orifice
s	static
th	throat

tot	total
w	wall
X	distance
0	zero burning time or start of burning
1, 2, 3 4, 5	instrumentation stations

Superscript:

*	reference condition

REFERENCES

1. Long, W. S.: The Determination of Coefficients of Heat Transfer to a Rocket Motor Nozzle by a Transient Method, pt. II. Rept. No. Tech. Note RPD 114, British RAE, Dec. 1954.
2. Anon.: Scale Model Heat Transfer Tests of the Nerva Nozzle - CY 1962. Rept. No. 2493, Aerojet General Corp., Apr. 1963.
3. Czeck, E. A.: Experimental Investigation of Heat Transfer to Nuclear Rocket Nozzles Using Shock Tube Techniques, Phase I and II. Rept. Nos. HM-1650-Y-1 & 2, Cornell Aero. Lab., Inc., 1962.
4. Fortini, Anthony; and Ehlers, Robert C.: Comparison of Experimental to Predicted Heat Transfer in a Bell-Shaped Nozzle with Upstream Disturbances. NASA TN D-1743, 1963.
5. Anon.: Space Programs Summary No. 37-25, Volume IV for the Period December 1, 1963 to January 31, 1964. Jet Prop. Lab., C. I. T., Feb. 29, 1964, p. 96.
6. Carslaw, H. S.; and Jaeger, J. C.: Conduction of Heat in Solids. Second ed., Oxford Univ. Press, 1959, pp. 304-306.
7. Lin, C. C.: Turbulent Flows and Heat Transfer. High Speed Aerodynamics and Jet Propulsion. Vol. V. Princeton Univ. Press, 1959, pp. 262-263.
8. Storm, M. L.: Heat Conduction in Simple Metals. J. Appl. Phys., vol. 22, no. 7, July 1951, pp. 940-951.
9. Zeleznik, Frank J.; and Gordon, Sanford: A General IBM 704 or 7090 Computer Program for Computation of Chemical Equilibrium Compositions, Rocket Performance, and Chapman-Jouguet Detonations. NASA TN D-1454, 1962.
10. Svehla, Roger A.: Thermodynamic and Transport Properties for the Hydrogen-Oxygen System. NASA SP 3011, 1964.
11. Eckert, E. R. G.; and Drake, Robert M., Jr.: Heat and Mass Transfer. McGraw-Hill Book Co., Inc., 1950.
12. Bartz, D. R.: A Simple Equation for Rapid Estimation of Rocket Nozzle Convective Heat Transfer Coefficients. Jet Prop. Lab., C. I. T., 1957, pp. 49-51.
13. Gordon, Sanford; and McBride, Bonnie J.: Theoretical Performance of Liquid Hydrogen with Liquid Oxygen as a Rocket Propellant. NASA MEMO 5-21-59E, 1959.

"The aeronautical and space activities of the United States shall be conducted so as to contribute . . . to the expansion of human knowledge of phenomena in the atmosphere and space. The Administration shall provide for the widest practicable and appropriate dissemination of information concerning its activities and the results thereof."

—NATIONAL AERONAUTICS AND SPACE ACT OF 1958

NASA SCIENTIFIC AND TECHNICAL PUBLICATIONS

TECHNICAL REPORTS: Scientific and technical information considered important, complete, and a lasting contribution to existing knowledge.

TECHNICAL NOTES: Information less broad in scope but nevertheless of importance as a contribution to existing knowledge.

TECHNICAL MEMORANDUMS: Information receiving limited distribution because of preliminary data, security classification, or other reasons.

CONTRACTOR REPORTS: Technical information generated in connection with a NASA contract or grant and released under NASA auspices.

TECHNICAL TRANSLATIONS: Information published in a foreign language considered to merit NASA distribution in English.

TECHNICAL REPRINTS: Information derived from NASA activities and initially published in the form of journal articles.

SPECIAL PUBLICATIONS: Information derived from or of value to NASA activities but not necessarily reporting the results of individual NASA-programmed scientific efforts. Publications include conference proceedings, monographs, data compilations, handbooks, sourcebooks, and special bibliographies.

Details on the availability of these publications may be obtained from:

SCIENTIFIC AND TECHNICAL INFORMATION DIVISION

NATIONAL AERONAUTICS AND SPACE ADMINISTRATION

Washington, D.C. 20546